J. Fluid Mech. (1992), *vol.* 238, *pp.* 277–296
Printed in Great Britain

Observations of fibre orientation in simple shear flow of semi-dilute suspensions

By CARL A. STOVER, DONALD L. KOCH AND CLAUDE COHEN

School of Chemical Engineering, Cornell University, Ithaca, NY 14853, USA

(Received 3 June 1991 and in revised form 21 October 1991)

The orientations of fibres in a semi-dilute, index-of-refraction-matched suspension in a Newtonian fluid were observed in a cylindrical Couette device. Even at the highest concentration ($nL^3 = 45$), the particles rotated around the vorticity axis, spending most of their time nearly aligned in the flow direction as they would do in a Jeffery orbit. The measured orbit-constant distributions were quite different from the dilute orbit-constant distributions measured by Anczurowski & Mason (1967*b*) and were described well by an anisotropic, weak rotary diffusion. The measured ϕ-distributions were found to be similar to Jeffery's solution. Here, ϕ is the meridian angle in the flow-gradient plane. The shear viscosities measured by Bibbo (1987) compared well with the values predicted by Shaqfeh & Fredrickson's theory (1990) using moments of the orientation distribution measured here.

1. Introduction

The orientation of fibres in simple shear flow plays an important role in determining the rheological properties of a suspension and the properties of composite materials produced by various forming operations. In the theoretical literature on fibre suspensions, the prediction of the suspension properties corresponding to a given suspension structure is better understood than the factors that control the structure itself. Thus, the goal of our investigation is to provide experimental evidence concerning the dynamic processes controlling fibre orientation in the simple shear flow of a semi-dilute suspension in a Newtonian fluid. A semi-dilute suspension is defined as one in which $nL^3 \gg 1$ and $nL^2d \ll 1$, where n is the number of fibres per unit volume, L is the fibre length and d its diameter. For $nL^3 \gg 1$, there are many particles interacting with any given fibre in the suspension at any point in time. The concentrations used in this study range from nL^3 of 1.0 to 45 for particle aspect ratios of 16.9 and 31.9, with the highest values of nL^2d being about 1.5.

Theoretical predictions are available for the stress in dilute and semi-dilute suspensions of non-Brownian high-aspect-ratio fibres with a known orientation distribution. These predictions are of the form (Batchelor 1971)

$$\sigma = \mu_{\text{fibre}}(\langle \boldsymbol{pppp} \rangle - \tfrac{1}{3}\delta\langle \boldsymbol{pp} \rangle) : \boldsymbol{E} + 2\mu \boldsymbol{E}, \tag{1.1}$$

where $\boldsymbol{p}$ is a unit vector parallel to the fibre axis of symmetry, $\boldsymbol{E}$ is the-rate-of-strain tensor, δ is the unit tensor, μ is the viscosity of the suspending fluid, μ_{fibre} is a function of concentration, orientation distribution, and fibre geometry, and the angle brackets represent an average over the orientation distribution of the fibres. This

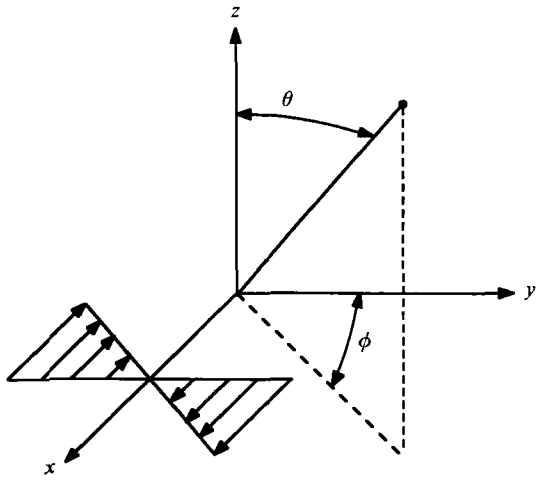

FIGURE 1. Definition of the spherical coordinate system for a fibre centred at the origin and subjected to an x, y simple shear.

prediction is valid provided that the fibre interactions are purely hydrodynamic and there is no fibre–fibre contact.

The expression for μ_{fibre} in the dilute limit was found by Batchelor (1971) to be

$$\mu_{\text{fibre}} = \frac{\pi n L^3 \mu}{6 \ln (2r_{\text{p}})} f(\epsilon), \tag{1.2}$$

where $\epsilon = [\ln (2r_{\text{p}})]^{-1}$ and r_{p} is the aspect ratio of the particle (length/diameter). For particles considered to be infinitely long and thin $f(\epsilon) = 1$, whereas the correction to $O(\epsilon^2)$ that accounts for the effects of finite aspect ratio is (Batchelor 1971)

$$f(\epsilon) = \frac{1+0.64\epsilon}{1-1.5\epsilon} + 1.659\epsilon^2. \tag{1.3}$$

Shaqfeh & Fredrickson (1990) have summed the particle interactions in the semi-dilute regime for long thin particles and shown that (1.1) is still applicable but μ_{fibre} is given by

$$\mu_{\text{fibre}} = \frac{\pi n L^3 \mu}{3[\ln (1/c) + \ln (\ln (1/c)) + A]}, \tag{1.4}$$

where c is the volume fraction of fibres, and $A = -0.66$ for a suspension in which all orientations are equally probable and $A = 0.16$ when all of the particles are aligned in a common direction. Corrections for (1.4) have not been developed to $O(\epsilon)$ or $O(\epsilon^2)$.

In order to use (1.1) for suspension rheology and comparable expressions for conduction (Shaqfeh 1988) and mechanical properties (Cates & Edwards 1984), one must know certain moments of the fibre orientation distribution. Theoretical predictions for the orientation distribution in the simple shear flow of a suspension of non-Brownian fibres are not yet available.

In 1922, Jeffery determined the motion of a single ellipsoidal particle in the Stokes flow of a Newtonian fluid. Bretherton (1962) showed that the same equations could be used to describe the motion of any axisymmetric particle provided that one used an effective aspect ratio r_{e} that is equal to the actual aspect ratio r_{p} for ellipsoidal

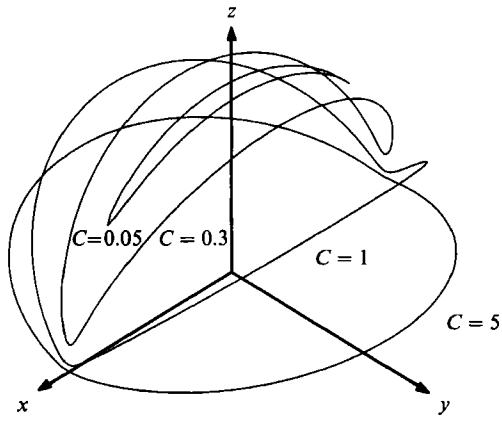

FIGURE 2. Jeffery orbits for $r_e = 22.3$ and various orbit constants for a simple shear in the (x, y)-plane.

particles, but must be determined experimentally for other particle shapes. The spherical coordinate system used to describe fibre orientation is defined in figure 1. The differential equations governing the time evolution of θ and ϕ are

$$\dot{\theta} = \frac{\dot{\gamma}(r_e^2-1)}{(r_e^2+1)} \sin\theta\cos\theta\sin\phi\cos\phi, \tag{1.5}$$

$$\dot{\phi} = \frac{\dot{\gamma}}{(r_e^2+1)}(r_e^2\cos^2\phi+\sin^2\phi), \tag{1.6}$$

where $\dot{\gamma}$ is the shear rate. Integration of (1.5) and (1.6) yields

$$\tan\theta = \frac{Cr_e}{(r_e^2\cos^2\phi+\sin^2\phi)^{\frac{1}{2}}}, \tag{1.7}$$

$$\tan\phi = r_e\tan\left(\frac{2\pi t}{T}+\kappa\right), \tag{1.8}$$

where C and κ are parameters known as the orbit constant and phase angle and $T = 2\pi(r_e+r_e^{-1})/\dot{\gamma}$ is the period of rotation of the fibre.

The motions described by (1.7) and (1.8) are illustrated in figure 2. If the fibre is centred at the origin in the figure, the end of the fibre sweeps out one of the orbits illustrated on the surface of the unit sphere. Each fibre rotates in a closed orbit parameterized by an orbit constant C that does not change for a fibre in a low-Reynolds-number flow of a Newtonian fluid unless effects such as inertia, Brownian forces, or fibre interactions take place. Equations (1.7) and (1.8) indicate that, for $C = O(1)$, the fibre spends a long time, of $O(r_e/\dot{\gamma})$, aligned in the (x, z)-plane and then quickly flips in an $O(1/\dot{\gamma})$ time through the rest of its orbit. On the other hand, fibres with an orbit constant of $O(1/r_e)$ wobble around the z-axis and never have a large component of their orientation in the y-direction. The tendency of fibres to spend most of the time near the (x, z)-plane has important rheological consequences. From (1.1), it can be seen that most arbitrarily chosen orientation distributions would produce an enhancement of the viscosity of $O(\epsilon nL^3\mu)$. However, only a fibre with an

$O(1)$ projection in the y-direction makes a large contribution to the shear stress, so the fibre contribution to the shear viscosity with orientation behaviour consistent with Jeffery's solution is actually only $O(\epsilon nL^2 d\mu)$.

Recently, progress has been made in describing the orientational dispersion caused by hydrodynamic interparticle interactions in two flow situations: the flow of freely suspended axisymmetric particles through a fixed bed of fibres or spheres (Shaqfeh & Koch 1988) and extensional flows of high-aspect-ratio particles in the dilute and semi-dilute regimes (Shaqfeh & Koch 1990). A comparable theory is not yet available for simple shear flow, but it is a subject of current research.

Anczurowski & Mason (1967*b*) observed fibre orientation in dilute suspensions of cylindrical fibres with $r_p = 18.4$ and $nL^3 = 0.016$, 0.066, and 0.26. For sufficiently small concentrations, the fibres would be expected to follow Jeffery orbits most of the time. The investigators determined the steady-state orbit-constant distribution in a Couette flow. The distributions were indistinguishable for the two lower concentrations, suggesting that these concentrations were in the dilute regime in which three-fibre interactions are rare. The fibres showed a pronounced shift towards low orbit constants relative to the orientation distribution that would arise if an initially isotropic suspension was sheared and the fibres remained in their initial orbit. We shall refer to the latter as the isotropic orbit distribution (Anczurowski & Mason 1967*a*). At the higher concentration, $nL^3 = 0.26$, the orbit distribution was shifted to higher orbit constants.

From the foregoing discussion, we can identify a number of important questions to be addressed by our experimental investigation. (i) Are the interactions in the semi-dilute regime strong enough to cause large deviations from Jeffery's rotation rate? (ii) Do the interactions cause fibres to flip more frequently, thereby increasing their projection in the gradient direction and their contribution to the stress? (iii) Is there any evidence for fibre–fibre contact in the semi-dilute regime? (iv) Does orientational diffusion serve as a useful model for the effects of fibre interactions? (v) Assuming that the fibres follow approximate Jeffery orbits, what is the distribution among the orbits?

To address these questions, we shall present measurements of the steady-state orientation distribution as well as some evidence of the transient changes in orientation in an index-or-refraction-matched, semi-dilute fibre suspension. Section 2 gives a brief description of the experimental apparatus and the fibre suspension. In §3.1 we present the results for the orbit-constant distribution, which is compared to an orientational diffusion model in §3.2. In §3.3, we examine the distribution for the meridian angle ϕ in the (x, y)-plane. The measured orientation distribution will be used together with (1.1) to make predictions for the effective shear viscosity that will be compared with the measurements of Bibbo (1987) in §3.4. The dynamics of orientation change will be addressed in §3.5.

2. Particle visualization apparatus

Anczurowski & Mason (1967*b*) sheared a suspension of cylindrical fibres with an aspect ratio $r_p = 18.4$ and concentrations, $nL^3 = 0.016$, 0.066, and 0.26 in a Couette device and measured the orbit constants of the suspended fibres in order to determine the orbit-constant distribution, $p(C)$. They used a particle-average method to calculate $p(C)$ by determining the orbit constant of about 500 different particles in a suspension undergoing shear. Both steady-state and transient C-distribution functions (Anczurowski, Cox & Mason 1967) were evaluated. Since relatively low

concentrations of fibres were utilized, opaque particles could be used without obscuring the particle being observed. The (x, z)-projection of the particles was observed and the maximum value of the angle θ, defined in figure 1, was determined from photographs. The value of the orbit constant was then determined from (1.7). Unfortunately the value of the orbit constant is quite sensitive to the maximum value of θ for $r_e \gg 1$ and $C > 1/r_e$, as can be seen from figure 2; therefore this method is not applicable to very large aspect ratios.

We also used a Couette device to generate a nearly simple shear flow. However, in order to investigate much more concentrated suspensions ($nL^3 = 1.0$–45) it was necessary to develop a system of non-sedimenting fibres in which the refractive index of the particles was nearly the same as the fluid (an isorefractive system) with a few opaque particles, the tracer fibres. A time-averaged distribution function $\psi(\phi, \theta)$ was measured by periodically observing the orientation of a tracer particle (θ, ϕ) allowing sufficient time for particle–particle interactions to occur between observations. The ergodic hypothesis implies that the time-averaged distributions and the particle-averaged distributions are equivalent if all the particles are assumed to be identical. Anczurowski & Mason (1967*b*) demonstrated that the ergodic hypothesis is satisfied by fibrous suspensions.

Folgar & Tucker (1974) reported experiments in which they measured the particle-average ϕ-distribution function of a semi-dilute suspension of opaque fibres in a Couette device. The angle ϕ was directly measured from viewing the projection of the particle in the (x, y)-plane. However, the centres of about 80% of the fibres were within $1.0L$ of a wall, which was shown by Stover & Cohen (1990) to be a region affected by the presence of the wall. In addition, it is suspected that the viewed particles were very close to the top free surface. Without an isorefractive suspension it would not be possible to view a particle from the z-direction unless it was very close ($< L$) to the top free surface at the concentrations studied by Folgar & Tucker.

A three-component fluid would be required to match the density and refractive index of an arbitrary material. Some of the constraints on the fluid components considered for this experiment are: high viscosity, so that a low Reynolds number can be attained; Newtonian behaviour; should not permeate polymethylmethacrylate (outer cylinder material) or the fibre material; low vapour pressure, so that the fluid composition remains constant; low toxicity. While three components are required in general, it was discovered that a two-component mixture of glycerine and polyethylene glycol (PEG) with a molecular weight of 600 (Union Carbide, Danbury, CT) could be used to match the density and nearly match the refractive index of cellulose acetate propionate, CAP (Tenite 357, Eastman Kodak Company, Rochester, NY). This material is not made into fibres on a commercial scale, but we found that CAP fibres of sufficient quality could be made in the laboratory. A mixture of glycerine (75.2 wt %) and PEG (24.8 wt %) at 25 °C matched the density of the CAP fibres (given as 1.222 g/cm^3) and had approximately the same refractive index as the fibres. The refractive index of the fluid was 1.4700 as measured with an Abbe refractometer while that of CAP was given as 1.4705. The shear viscosity of the fluid was measured with a Haake viscometer to be approximately 10 P.

CAP in pellet form was melted and extruded through a circular die using a capillary rheometer (Sieglaff-Mckelvey, Philadelphia, Pennsylvania) on constant-velocity mode, and the continuous strand of fibre produced was collected onto a spool rotating at a constant speed. The resulting spool of fibre was cut into equal lengths by using a device that we designed and built especially for this purpose. A length of fibre was wrapped around an aluminium plate so that the fibres did not overlap. A

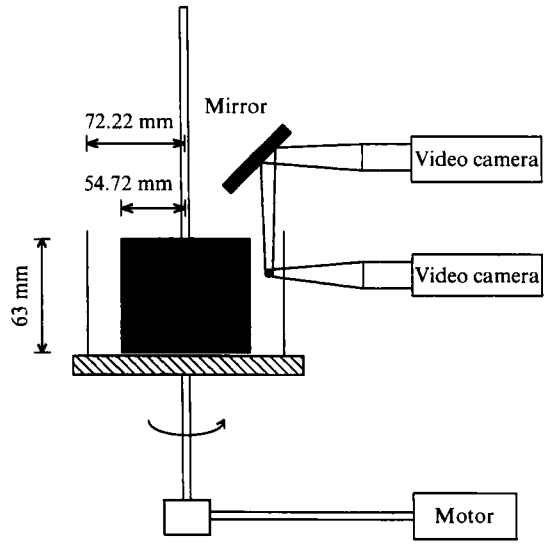

FIGURE 3. Schematic of the Couette device.

special fixture holding 50 parallel and equally spaced blades was used to cut the fibres by using a hydraulic press to push the blades and base together. In this way, several thousand fibres could be cut at a time. Two sizes were produced for the experiments: for the high-aspect-ratio fibres, $L = 2.68$ mm, $d = 84$ μm, and $r_p = 31.9$ with a standard deviation for r_p of 2.73; for the low-aspect-ratio fibres, $L = 1.61$ mm, $d = 95$ μm, and $r_p = 16.9$ with a standard deviation of 2.78. Measurements of size distributions were made under a microscope by constructing histograms of 100 particles. Tracer fibres with the same density were made by the same method from black CAP, also supplied by Kodak.

Figure 3 shows a schematic of the Couette apparatus constructed for this study. The inner radius was $r_i = 5.472$ cm, the outer Couette radius was $r_o = 7.222$ cm. The inner cylinder was held fixed while the outer cylinder rotated at a constant rate. Each time the tracer fibre passed through the volume that was being viewed by the video cameras, two images of the fibre were recorded, superimposed on a timer. Observations of the tracer particle were made only when the centre of the fibre was more than 2 fibre lengths from interfaces, which was shown by Stover & Cohen (1990) to be a region free from wall effects. The Reynolds number based on particle length was at most 0.003, which was shown by Karnis, Goldsmith & Mason (1966) to be sufficiently small that inertia would be unimportant on the timescale of our observations. The experiments were performed in a constant-temperature laboratory which was kept at 25 °C ± 0.5 °C.

A moderate value of 4 was chosen for the ratio of the height of the Couette device to the gap between the cylinders, in order to minimize the number of fibres that had to be produced by hand. For this geometry, a weak secondary flow with an amplitude about 10^{-4} smaller than the primary cylindrical Couette flow was present. It was experimentally determined that the rotation of a fibre about $2L$ from the top surface showed no evidence of shear in the z-direction, indicating that the weak secondary flow did not cause a measurable effect on fibre orientation. However, over the long time period of several hours, the secondary flow could convect a fibre from a region where wall effects were important into the observation region at the centre of the

gap. Since the time over which a fibre's orientation remains correlated increases with decreasing concentration (cf. §3.5), this sets a lower bound of $nL^3 \approx 0.5$ on the fibre concentration for which we could obtain reliable measurements. An attempt to decrease the amplitude of the secondary flow by using an inviscid fluid (mercury) at the bottom of the suspension to achieve a free-surface boundary condition was unsuccessful, because a rigid layer of unknown structure or substance formed at the interface between the mercury and PEG/glycerin mixture.

In order to facilitate the measurement of the orientation of the two recorded fibre images, simple image analysis techniques were used. After the experiment was completed and many images had been recorded on video tape, a frame grabber (Data Translation Corp., Marlboro, MA) was used to digitize a frame of video information in which the images of the fibre were in the centre of the screen. Simple routines were then used to display this image on a monitor as a still frame. A program was written to use a mouse (Microsoft Corp., Redmond, WA) so that lines could be superimposed on the image of the fibre. Two lines were drawn, using the mouse, parallel to the images of the fibre, and the slopes were calculated and automatically recorded in a data file. The time was recorded from the frame and also written into the data file. Later, the data in the file were analysed, and the orientation of the particle was calculated. Corrections were made to take into account the misalignment of the picture frame from the flow coordinates and the distortion of the picture due to unequal magnification of the axes.

3. Results and discussion

3.1. *The orbit-constant distribution*

The average shear rate experienced by the tracer particle, the average time between observations (the observation period), and the number of observations made for each suspension are shown in table 1, along with other experimental parameters and results. The shear rate at the centre of the fibre was calculated on the basis of the flow field generated between the two concentric cylinders of our device, and the radial position of the particle was calculated from its average velocity. Stover & Cohen (1990) have shown that a parabolic flow field does not affect the orientation dynamics of a fibre, and we expect that the small nonlinearity of our flow field will have a negligible effect.

A direct observation of the tracer particle in the semi-dilute suspensions indicated that the particle tended to rotate around the vorticity axis, spending a fraction of time of about $(1-1/r_e)$ nearly aligned with the (x,z)-plane as it would in a Jeffery orbit. However, the period of rotation was not uniform and at times the particles rotated for a small time in the opposite direction of the mean rotation. Later it will be shown that the quantitative differences in the ϕ-distribution for Jeffery's result and our observations are rather small. The qualitative observation that fibre rotation in a semi-dilute suspension is similar to Jeffery orbits is consistent with the theoretical calculation of Koch & Shaqfeh (1990). This calculation showed that many-fibre interactions in a semi-dilute suspension cause a small ($< 10\%$) deviation of the average rotation rate from Jeffery's result.

When representing the orbit-constant distribution, it is advantageous to plot the quantity $C/(C+1)$ since its value is bound between zero and one. This quantity will be referred to as C_b. The steady C_b-distribution measured for $r_p = 18.4$ and $nL^3 = 0.016$ (Anczurowski & Mason 1967*b*), which was shown to be in the dilute regime, is illustrated in figure 4(*a*). The symbols represent the experimental measurements, the

r_p	nL^3	No. of observations	Ave. shear rate (s^{-1})	Observation period (s)	$\langle p_1^2 p_2^2 \rangle$	ϕ_{shift} (deg.)	ϕ_{dev} (deg.)	$D_{\theta\theta}/D_{\phi\phi}$ best fit value
16.9	20	616	0.319	82.8	0.0222	−1.00	13.60	2.53
16.9	10	599	0.368	79.3	0.0278	−0.0770	15.39	1.21
16.9	3.0	1334	0.459	76.5	0.0249	0.684	13.68	1.37
16.9	1.0	2356	0.471	82.5	0.0275	0.0320	13.42	1.22
31.9	45	472	0.472	84.6	0.0115	−0.961	7.59	3.16
31.9	18	963	0.478	81.6	0.0115	−1.83	7.48	1.38
31.9	10	1177	0.451	76.2	0.0114	−1.41	7.44	2.85
31.9	5.0	1412	0.447	73.7	0.0116	−1.85	7.05	2.18

TABLE 1. Some experimental parameters

dotted line is the isotropic C_b-distribution, and the solid line is the best fit of the data by the rotary diffusion model that will be discussed below. Two-body interactions have the net effect of producing a C_b-distribution that favours low orbit constants relative to the isotropic C-distribution. As can be seen in figure 2, these orbits rotate around the z-axis but never have a large projection in the gradient direction.

Figure 4(*b*) shows the measured C_b-distribution for $r_p = 31.9$ and $nL^3 = 45$ compared with the isotropic C-distribution and the rotary diffusion model. The measured C_b-distributions for the eight semi-dilute suspensions in our study are all qualitatively similar, with higher orbit constants being favoured relative to the dilute C_b-distribution. The error bars are 80% confidence intervals and were calculated in the following manner. In calculating the uncertainty for our experiments, it was necessary to take account of the temporal correlations in our data, because the observation time was shorter than the time over which a fibre's orientation became uncorrelated due to fibre interactions. We divided the observations into groups of 50, maintaining chronological order, and performed a t-test in order to determine the variation of $p(C_b)$ from group to group (Stover 1991). In all cases the approximate time over which orientations remained correlated (discussed in §3.5) was much smaller than the group size. The error bars estimated by this method were found to be insensitive to the group size.

3.2. *Rotary diffusion model*

The steady orientation-distribution function for fibres in a simple shear flow has not yet been determined theoretically. However, in the semi-dilute regime, there is a strong indication that fibre–fibre interactions are purely hydrodynamic and that changes in orientation due to mechanical contact between fibres are not significant. Evans (1975) showed that slender fibres following Jeffery orbits in shear flow do not collide regardless of the interparticle separation. This is a result of the nature of the Jeffery orbits for large aspect ratios, which describe the motion of a fibre to be similar to that of a material line except that the fibre resists stretching. The combination of particle rotation and translation causes particles to pass by each other without making contact. In addition, Evans showed that the hydrodynamic interactions between a pair of fibres calculated from slender-body theory do not cause fibres to collide. Koch & Shaqfeh (1990) solved for the average rotation rate for infinite-aspect-ratio particles in the semi-dilute regime. They found that the rotation rate was slowed by 10% at most, relative to Jeffery's rotation rate, and there was no

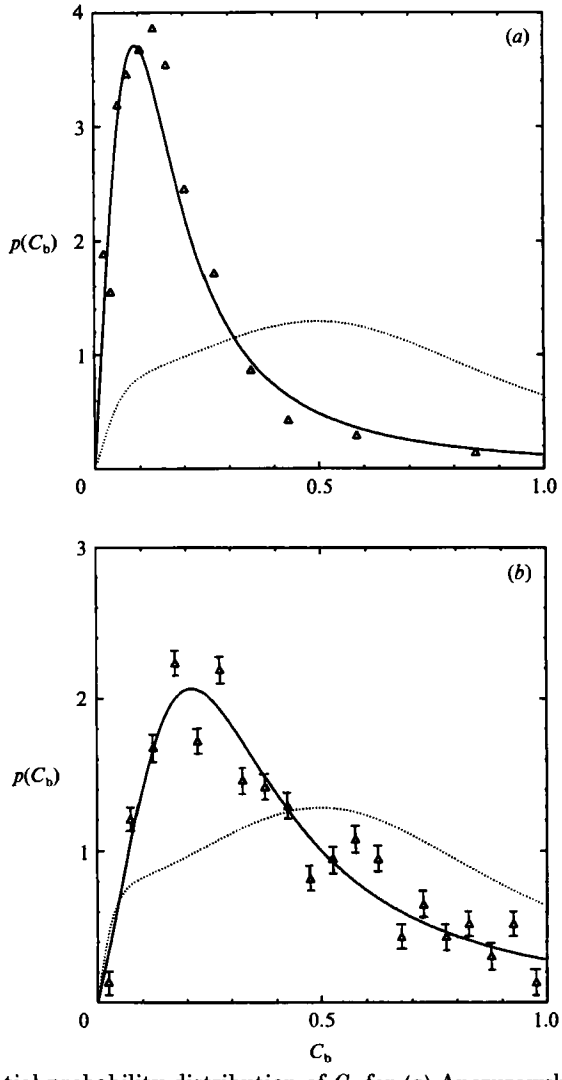

FIGURE 4. Differential probability distribution of C_b for (*a*) Anczurowski & Mason's (1967*b*) data for $r_p = 18.4$ and $nL^3 = 0.016$, and (*b*) for our experiments with $r_p = 31.9$ and $nL^3 = 45$. The solid line is the best fit to (3.2) with a variable $D_{\theta\theta}/D_{\phi\phi}$. The dotted line is the isotropic distribution function. The error bars are 80 % confidence intervals.

difference from the Jeffery orbit when the fibre was aligned with either the flow direction or the velocity gradient. The authors argued that this modest correction would not cause particles to collide at a frequency that would dominate the hydrodynamic interactions.

Recent work by Shaqfeh & Koch (1988, 1990) has made theoretical predictions concerning the orientational dispersion of fibres caused by hydrodynamic interactions. Shaqfeh & Koch (1988) found that an effective diffusivity could be used to describe the effects of hydrodynamic interactions on the orientation of axisymmetric particles flowing through a fixed bed. However, it was necessary to take account of the dependence of the diffusivity on fibre orientation and the associated orientational drift velocity, in order to predict the orientation distribution. The resulting theoretical predictions were confirmed by the experiments of Frattini *et al.* (1991).

Shaqfeh & Koch (1990) found that the orientational dispersion caused by fibre interactions in extensional flow was non-local, but the authors were nonetheless able to make predictions concerning moments of the orientation distribution.

From the aforementioned studies, it is clear that the concept of a hydrodynamically induced rotary diffusion is useful in describing hydrodynamic interactions. However, the theoretical description may be complicated by the dependence of the diffusivity on fibre orientation, orientational drift, and non-local effects. In the absence of a theory for orientational dispersion in simple shear flows, we will adopt the simplest diffusive model for the interactions that can describe the orbit distribution.

The rotary diffusion problem is posed in terms of the probability distribution function, $\psi(\phi, \theta)$. Burgers (1938) derived the general equation governing the time variations of $\psi(\phi, \theta)$. Presented in terms of a tensorial rotary diffusion, the equation is

$$\frac{\partial \psi(\phi,\theta)}{\partial \tau} = -\nabla_p \cdot (\dot{\boldsymbol{p}}(\phi,\theta)\,\psi(\phi,\theta)) + \nabla_p \cdot \boldsymbol{D}_{\mathrm{r}} \cdot \nabla_p \psi(\phi,\theta), \tag{3.1}$$

where $\dot{\boldsymbol{p}}(\phi, \theta)$ is the angular velocity described by Jeffery's equations and $\boldsymbol{D}_{\mathrm{r}}$ is the rotary diffusivity.

In order to develop a solution for a determinate steady-state distribution, Leal & Hinch (1971) considered the problem of how a scalar rotary diffusivity (i.e. a rotary Brownian motion) determines the C-distribution function for fibres obeying Jeffery's equations in the limit as the rotary diffusivity goes to zero. The solution method begins by stipulating that at steady state the net flux of particles across any particular orbit is zero. The ϕ-distribution function is unchanged by a weak rotary diffusivity since the Jeffery convective term in the ϕ-direction is non-zero. While Leal & Hinch's principal focus was on slightly Brownian fibres, they also compared their steady-state C-distributions to Anczurowski & Mason's (1967*b*) experimental data for dilute suspensions to see if fibre–fibre interactions for non-Brownian particles could be modelled by a rotary diffusivity. The C-distributions differed considerably, and they concluded that either infrequent strong interactions were important to this problem or distant interactions were described poorly by a rotary diffusivity.

Since the imposed flow field and the resulting orientation distribution function are anisotropic, there is no reason to expect that an isotropic diffusivity would be able to account for fibre–fibre interactions. Rahnama *et al.* (1992) have extended Leal & Hinch's solution to account for a weak, anisotropic rotary diffusivity, with different diffusivities in the θ- and ϕ-directions, $D_{\theta\theta}$ and $D_{\phi\phi}$. For example, $D_{\theta\theta}$ is the proportionality between gradients of $\psi(\phi, \theta)$ in the θ-direction and the flux of probability in the θ-direction. The resulting steady-state orbit-constant distribution, in the limit of large aspect ratio, is given by

$$p(C_{\mathrm{b}}) = \frac{4C_{\mathrm{b}}(D_{\theta\theta}/D_{\phi\phi})}{\left(4\left[\dfrac{C_{\mathrm{b}}}{1-C_{\mathrm{b}}}\right]^2 \dfrac{D_{\theta\theta}}{D_{\phi\phi}} + 1\right)^{\frac{3}{2}} (1-C_{\mathrm{b}})^3}. \tag{3.2}$$

Figure 4 shows our experimental data for $r_{\mathrm{p}} = 31.9$ and $nL^3 = 45$ and Anczurowski & Mason's (1967*b*) dilute experiments compared to Rahnama *et al.*'s (1992) theory for the value of $D_{\theta\theta}/D_{\phi\phi}$ which gives a best fit. The agreement is quite good, with the theoretical curve lying within the error bars for figure 4(*b*). Note especially the comparison in figure 4(*a*) for the dilute limit, with $D_{\theta\theta}/D_{\phi\phi} = 16.23$, in which the peak

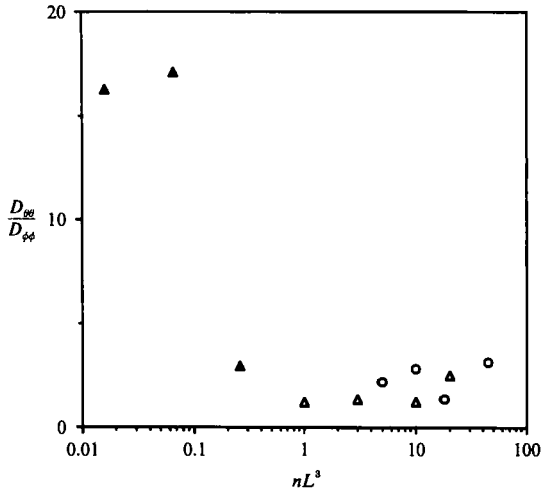

FIGURE 5. Values of $D_{\theta\theta}/D_{\phi\phi}$ found by a best fit of the anisotropic, weak rotary diffusion model: ▲, Anczurowski & Mason's (1967*b*) data for $r_p = 18.4$; △, for $r_p = 16.9$; and ○, for $r_p = 31.9$.

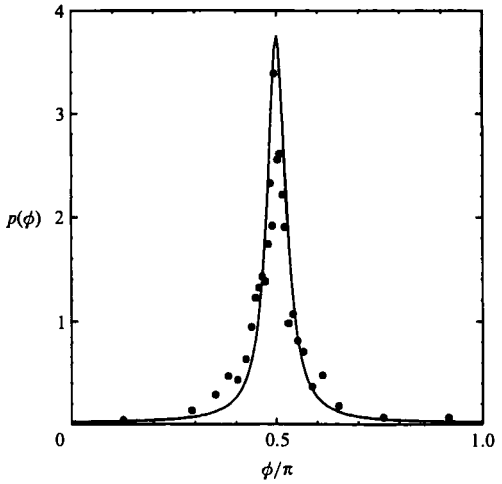

FIGURE 6. The experimental ϕ-distribution for $r_p = 16.9$ and $nL^3 = 20$ (○), and Jeffery's result for a particle with the same $r_e = 0.7r_p$ (——).

and spread of this dilute experiment are described very well by this one-parameter fit. All of the other experimental data obtained were fit by this anisotropic, weak rotary diffusion model equally well.

Figure 5 shows a plot of the best-fit value of $D_{\theta\theta}/D_{\phi\phi}$ compared to nL^3 for our experiments and Anczurowski & Mason's (1967*b*) data. The best-fit values of $D_{\theta\theta}/D_{\phi\phi}$ are shown in table 1. The low-aspect-ratio particles ($r_p = 16.9$ for our experiments and $r_p = 18.4$ for Anczurowski & Mason's) show a plateau at about $D_{\theta\theta}/D_{\phi\phi} = 17$ for the two lowest concentrations, the apparent dilute regime. This is followed by a steep drop to another plateau, at about $D_{\theta\theta}/D_{\phi\phi} = 1.5$, in the semi-dilute regime. The higher-aspect-ratio particles also show a semi-dilute plateau with $D_{\theta\theta}/D_{\phi\phi}$ around 1.5. A comparison of figure 4(*b*) including the error bars with similar plots for the other experiments showed little or no statistical significance for the variations of $D_{\theta\theta}/D_{\phi\phi}$ with nL^3 and r_p in the semi-dilute regime.

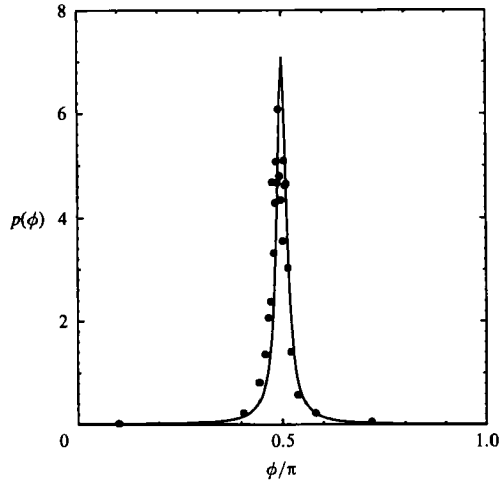

FIGURE 7. As figure 6 but for $r_p = 31.9$ and $nL^3 = 45$.

3.3. *The ϕ-distribution function*

The measured ϕ-distribution functions for the suspensions with $r_p = 16.9$ and $nL^3 = 10$, and with $r_p = 31.9$ and $nL^3 = 45$ are shown in figures 6 and 7, respectively. The symbols represent the experimental data and the line is Jeffery's result with $r_e = 0.7r_p$, which is the relationship between r_e and r_p originally found by Trevelyan & Mason (1951) for cylindrical fibres with aspect ratios in this range. None of the measured ϕ-distributions differ greatly from Jeffery's solution, with only a small amount of spreading or shifting of the distribution being evident.

It can be shown that, if all particle–particle interactions are hydrodynamic, the ϕ-distribution must be symmetric about the flow direction ($\phi = \frac{1}{2}\pi$). The argument follows from the form of the N-particle Smoluchowski equation and is similar to that given by Koch (1989) for the pair probability in a suspension of spheres. The Smoluchowski equation is

$$\sum_{N=1}^{\infty} \nabla_{R_i} \cdot (U_i P) + \nabla_{p_i} \cdot (\dot{p}_i P) = 0, \tag{3.3}$$

where $P(\boldsymbol{R}_1 \ldots \boldsymbol{R}_N; \boldsymbol{p}_1 \ldots \boldsymbol{p}_N)$ is the probability of a certain configuration, $\boldsymbol{U}_i$ is the velocity of the ith particle, $\boldsymbol{p}_i$ is the orientation of the ith particle, and $\boldsymbol{R}_i$ is the position of the ith particle. The quantities $\boldsymbol{U}_i$ and $\dot{\boldsymbol{p}}_i$ are linear in $\dot{\gamma}$ so that P is unchanged if the flow is reversed. Therefore, the ϕ-distribution must be symmetric upon reflection through the (x, z)-plane.

A finite effective diffusivity would not yield results that are consistent with the symmetry noted above; instead it would give a distribution whose peak is shifted from the x-direction ($\phi = \frac{1}{2}\pi$) to a value of ϕ less than $\frac{1}{2}\pi$ (Stover 1991). This indicates that a complete description of hydrodynamic interactions is more sophisticated than the simple anisotropic diffusion model used in §3.2 to fit the orbit-constant distribution. Although the anisotropic diffusion model gives a good fit to the data of $p(C_b)$, it fails to describe $P(\phi)$.

In order to quantify the amount of spreading and shifting of the ϕ-distributions, we define ϕ_{shift} as the average of $(\phi - \frac{1}{2}\pi)$, i.e. the difference between the average value of ϕ and the flow direction, and ϕ_{dev} as the average of the absolute value of $(\phi - \frac{1}{2}\pi - \phi_{shift})$, i.e. the average deviation from the average orientation. In figure 8

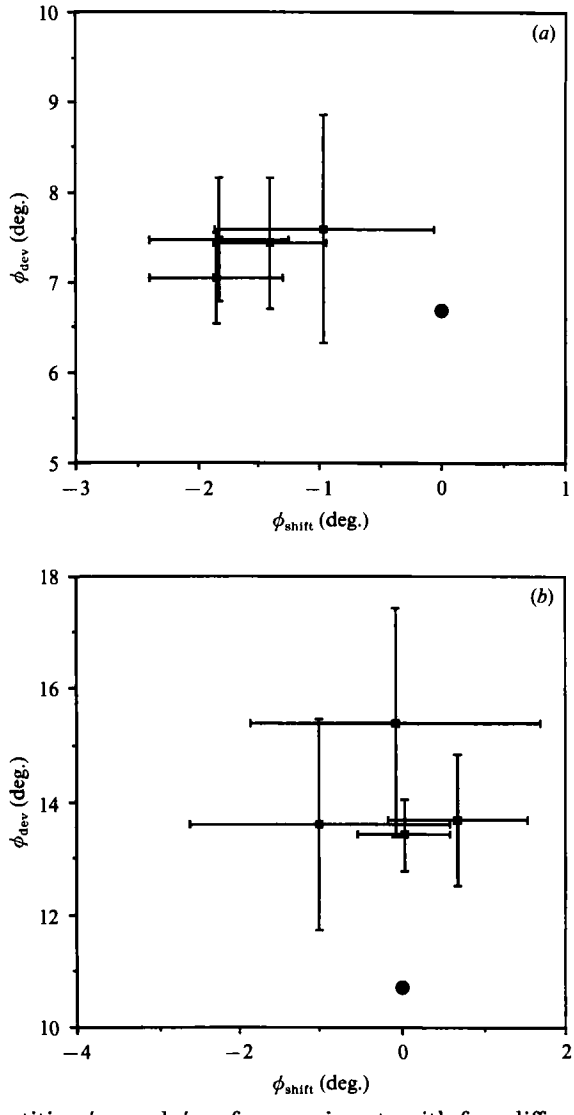

FIGURE 8. The quantities ϕ_{dev} and ϕ_{shift} for experiments with four different concentrations for (*a*) $r_p = 31.9$ and (*b*) $r_p = 16.9$: ■, the experimental values with the error bars being 80% confidence intervals; ●, Jeffery's result for a particle with the same effective aspect ratio.

values of ϕ_{dev} and ϕ_{shift} for various concentrations and aspect ratios are compared to a point representing Jeffery's solution for particles with the same effective aspect ratio. The error bars shown are 80% confidence intervals calculated by the method described above.

For $r_p = 16.9$, it appears that there is no significant shifting of the ϕ-distribution, but 2° to 3° of spreading of the distribution with no relationship between ϕ_{dev} and nL^3 being noted. For $r_p = 31.9$, there seems to be no statistically significant spreading of the distribution but the distribution peak is shifted by 1° to 2° below $\phi = \frac{1}{2}\pi$. If all of the interactions are hydrodynamic as postulated, there should be no shifting of the ϕ-distribution, and the source of its apparent shifting for the high-aspect-ratio particles is unknown. For both aspect ratios, there is no systematic change in ϕ_{shift} or ϕ_{dev} with concentration.

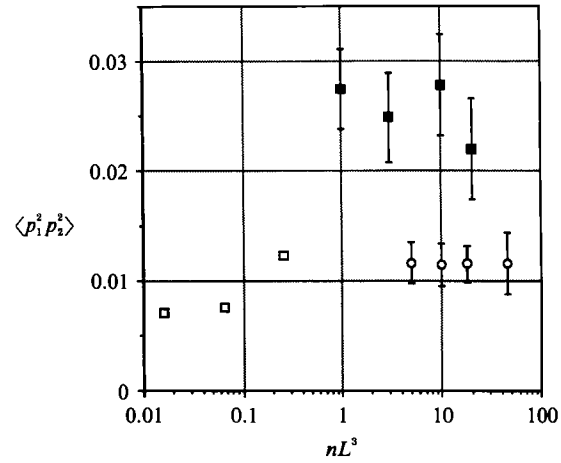

FIGURE 9. Values of $\langle p_1^2 p_2^2 \rangle$ obtained from experimental data as a function of concentration: □, estimated from Anczurowski & Mason's (1967*b*) data for $r_p = 18.4$; ■, for $r_p = 16.9$; and ○, for $r_p = 31.9$.

A polydisperse distribution of aspect ratios can affect the ϕ-distribution since the angular velocity in the ϕ-direction is a function of r_e. The ϕ-distribution for a distribution of aspect ratios was calculated assuming that the r_p-distributions are Gaussian with the standard deviations given above. For both aspect ratios, the resulting ϕ-distributions were nearly identical to the one calculated assuming a monodisperse r_p-distribution. Therefore, none of the observed spreading can be attributed to the distribution of aspect ratios.

Folgar & Tucker (1984) used a rotary diffusivity and an infinite-aspect-ratio Jeffery rotation rate in the (x, y)-plane to describe their observed $P(\phi)$ distributions. Since most of the spread in our $P(\phi)$ distributions can be attributed to the finite aspect ratio of the particles, Folgar & Tucker's procedure would lead to a substantial overestimate of the effects of fibre interactions.

3.4. *Rheology of fibrous suspensions*

When boundary effects are negligible, an effective shear viscosity can be defined along with effective normal stress coefficients. The effective viscosity of both the dilute and semi-dilute regimes is expected to be the result of a purely hydrodynamic stress and can be seen from (1.1) to be a function of the $\langle p_1^2 p_2^2 \rangle$ component of the quadrad $\langle \boldsymbol{pppp} \rangle$, where the subscripts 1 and 2 refer to the flow and gradient directions, respectively. It is given by

$$\mu_{\text{rel}} = 1 + \frac{\mu_{\text{fibre}}}{\mu} \langle p_1^2 p_2^2 \rangle, \tag{3.4}$$

where μ_{rel} is the relative viscosity, which is the ratio of suspension viscosity to the continuous-phase viscosity, and μ_{fibre} is determined by (1.2) for the dilute limit and by (1.4) for the semi-dilute limit. In (1.4) we are using the fully aligned option which should be fairly accurate since the deviation of fibre orientation from the flow direction is small, like $O(1/r_e)$. The observation that particles execute approximate Jeffery orbits in the semi-dilute regime supports the hypothesis that the stress is purely hydrodynamic.

Figure 9 shows $\langle p_1^2 p_2^2 \rangle$ as a function of nL^3 for our experiments as well as those of Anczurowski & Mason (1967*b*). For the low-aspect-ratio particles ($r_p = 18.4$ for

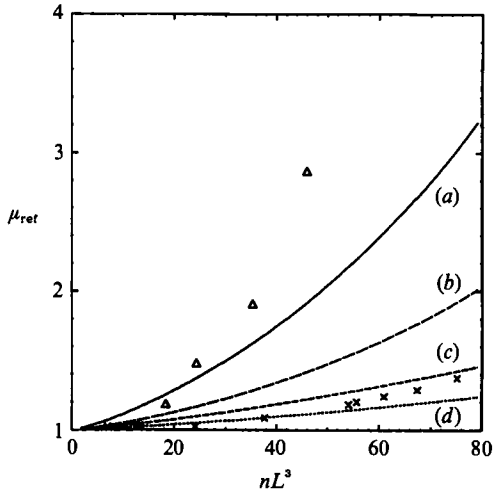

FIGURE 10. The relative viscosity, μ_{rel}, as a function of nL^3, from Bibbo's (1987) experiments: △, $r_p = 17$; and ×, $r_p = 33$; (*b*) and (*d*) are for the semi-dilute theory for $r_p = 17$ and 33 respectively; (*a*) and (*c*) are as (*b*) and (*d*) respectively, but using the factor calculated for the effect of finite-aspect-ratio particles in the dilute regime.

Anczurowski & Mason and $r_p = 16.9$ for this work) there is a dilute plateau at about $\langle p_1^2 p_2^2 \rangle = 0.007$ for the two lowest concentrations and a semi-dilute plateau at about $\langle p_1^2 p_2^2 \rangle = 0.025$ with $nL^3 = 0.26$ bridging the two regimes. Within these two plateaux each data point lies within the error bars of the other points. For the high-aspect-ratio particles ($r_p = 31.9$) there is a semi-dilute plateau with all the values of $\langle p_1^2 p_2^2 \rangle$ being within 1% of 0.0115. The error bars are 80% confidence intervals calculated as before. The factor of three increase in $\langle p_1^2 p_2^2 \rangle$ between the dilute and semi-dilute region is almost exclusively due to changes in the C-distribution since the ϕ-distributions are only slightly different from Jeffery's result.

Bibbo (1987) has measured the effective viscosity of fibrous suspensions with nearly the same r_p as those used in this investigation, using a torsion cup, which is a parallel-plate rheometer with a wall attached to the outer edge of the lower plate, to hold the suspension in place. Care was taken to ensure that the two plates were sufficiently separated so as to measure a true effective viscosity. This condition was not met by many other studies in the literature. In figure 10, the symbols represent the experimental measurements of the continuum shear viscosity by Bibbo (1987) for $r_p = 17$ and 33. Experiments conducted by Ganani & Powell (1986) also measured the true effective viscosity using particles where $r_p = 24.3$. Their data fall approximately midway between the two experimental curves shown here.

Curves (*b*) and (*d*) on figure 10 show the theoretical predictions obtained from (1.4), using our measured orientation distribution. This theory does not include the effect of finite-aspect-ratio particles and appears to underpredict the effective viscosity by a factor of about two. There is no semi-dilute theory available that is correct to $O(\epsilon)$ or $O(\epsilon^2)$. In the dilute regime for particles with $r_p \approx 20$, the effect of including terms that account for the finite-aspect-ratio effects to $O(\epsilon^2)$ rather than the infinite-aspect-ratio theory is to increase the viscosity by a factor of about two, see (1.2) and (1.3). This factor calculated for the dilute regime is considered here for the semi-dilute case since there is no similar theory for the semi-dilute regime. This concept has already been employed with success by Mewis & Metzner (1974) for the study of elongational viscosity. The μ_{rel} given by (3.4) for the semi-dilute regime multiplied by $f(\epsilon)$ for the

dilute regime given by (1.3) gives curves (*a*) and (*c*) in figure 10. The comparison to the data is reasonably good, underpredicting the data slightly for the low-aspect-ratio particles and overpredicting for those of high aspect ratio. Note that the enhancement of the effective viscosity is rather modest, because the weakness of the interactions gives an $O(nL^2d)$ fibre stress which is characteristic of fibres in Jeffery orbits.

From (1.1) it can be shown that the effective normal stress differences in the semi-dilute regime are given by

$$\sigma_{11}-\sigma_{22} = \mu_{\text{fibre}}\,\dot{\gamma}(\langle p_1^3 p_2\rangle - \langle p_2^3 p_1\rangle), \tag{3.5}$$

$$\sigma_{22}-\sigma_{33} = \mu_{\text{fibre}}\,\dot{\gamma}(\langle p_2^3 p_1\rangle - \langle p_1 p_2 p_3^2\rangle). \tag{3.6}$$

The first and second normal stress differences are predicted to be proportional to $\dot{\gamma}$, unlike many polymeric fluids in which the normal stress differences are proportional to $\dot{\gamma}^2$. The three moments appearing in (3.5) and (3.6) are all zero if the orientation-distribution function is symmetric with respect to the (x,z)-plane, which is the case in the absence of particle–particle interactions or if particle–particle interactions are purely hydrodynamic. Potentially, normal stress differences could be sensitive measures of non-symmetric changes in the ϕ-distribution function. These moments were calculated from the experimental data. In the cases where they were non-zero, mostly for the large-aspect-ratio particles, the predicted normal stress was too small to be measured by standard rheological techniques. In fact, Bibbo (1987) found that the transient normal stress difference was indeed proportional to $\dot{\gamma}$, but that at steady state the measured normal force was below the sensitivity of the rheometer.

3.5. *Transient orientation distributions*

Since time-averaged data were collected for our study, the transient orientation distribution $\psi(\phi,\theta,t)$ cannot be calculated. However, by studying the time correlation function of an orientation parameter some aspects of the transient distribution function can be investigated. During the experiment, the orientation of the tracer particle is observed as it passes a fixed point with only the outer cylinder rotating. The nth observation is related to the $(n-1)$th observation and to a lesser degree the $(n-2)$th. The rate of change of orientation depends on the concentration of the suspension since the rate and nature of interactions is a function of nL^3. Figure 11 shows the value of C_b as a function of the number of particle circuits for $r_p = 16.9$ and $nL^3 = 1.0$ and 20. For the low-concentration case, C_b is a strong function of its previous value, changing by a relatively small amount from one observation to the next, while for the high-concentration case the orientation is nearly independent of its history.

The function $\langle C_b(t)\,C_b(t-\tau)\rangle$ is defined as the time correlation function of $C_b(t)$, where τ is the delay time, t is the time measured during the experiment, and the angle brackets denote averages over all available values. For $\tau = 0$, $\langle C_b(t)\,C_b(t-\tau)\rangle = \langle C_b(t)^2\rangle$ and as $\tau\to\infty$, the orbit constant becomes statistically uncorrelated and $\langle C_b(t)\,C_b(t-\tau)\rangle = \langle C_b(t)\rangle^2$. By analysing the decay of $\langle C_b(t)\,C_b(t-\tau)\rangle$ as a function of τ, the temporal stochastic fluctuations of $C_b(t)$ can be explored. For the case of fibres suspended in a shear flow, the transient rotary diffusion problem has been investigated for a strong rotary diffusivity (Cohen & Leal 1978; Rallison & Leal 1981; Stasiak & Cohen 1983), but the transient weak rotary diffusivity has not been studied. Since the fibre–fibre interactions observed in this work have been successfully modelled with a weak rotary diffusivity, there is thus no theoretical prediction to compare with the observed time correlation function.

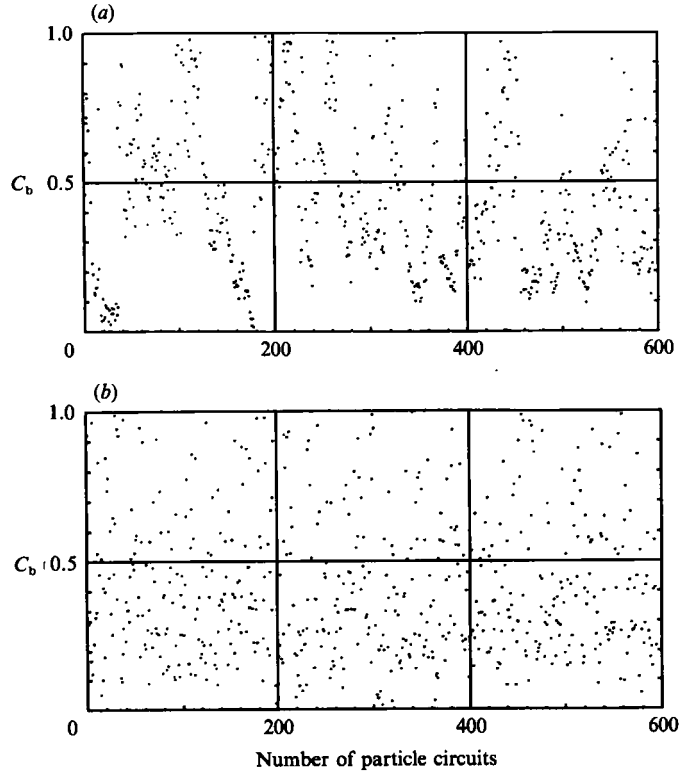

FIGURE 11. The quantity C_b as a function of the number of particle circuits for (*a*) $nL^3 = 1.0$ and (*b*) $nL^3 = 20$, with $r_p = 16.9$.

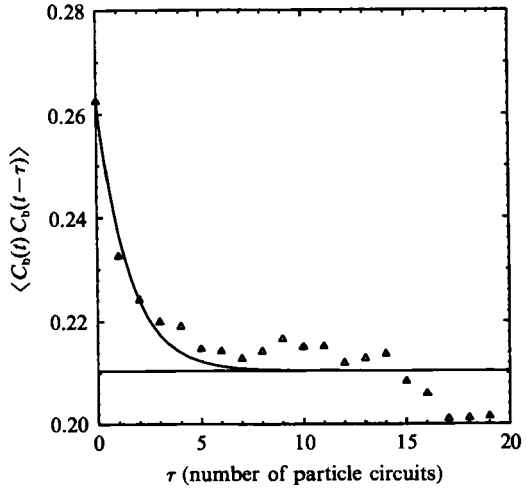

FIGURE 12. The time correlation function, $\langle C_b(t)\, C_b(t-\tau)\rangle$, for $r_p = 16.9$ and $nL^3 = 10$ fit to an exponential decay with $\tau_c \dot{\gamma} = 30.5$.

Figure 12 shows the time correlation function of $C_b(t)$ for $r_p = 16.9$ and $nL^3 = 10$, with τ measured in the number of particle circuits. The uncertainty in the data for this correlation function increases with τ, since the average is taken over a smaller number of orbit-constant products for larger time intervals, owing to the finite

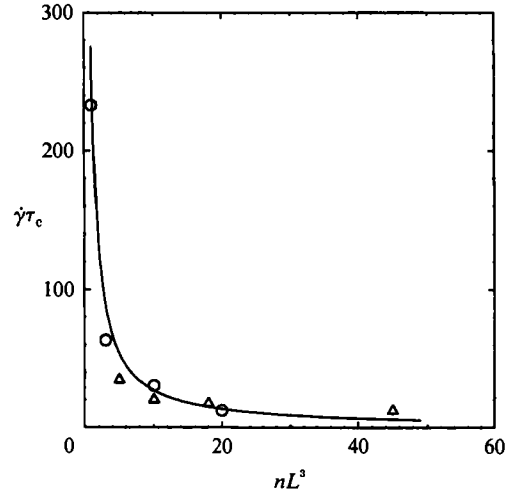

FIGURE 13. The correlation time, τ_c, versus nL^3 for the experiments compared to a best fit, $\dot{\gamma}\tau_c = 270/nL^3$: ○, $r_p = 16.9$; and △, $r_p = 31.9$.

r_p	nL^3	$\langle C_b(t)^2\rangle$	$\langle C_b(t)\rangle^2$	Correlation time: $\tau_c\dot{\gamma}$
16.9	20	0.226	0.168	12.5
16.9	10	0.263	0.211	30.5
16.9	3.0	0.261	0.207	63.3
16.9	1.0	0.292	0.234	233
31.9	45	0.205	0.150	12.3
31.9	18	0.272	0.214	17.6
31.9	10	0.206	0.151	20.2
31.9	5.0	0.232	0.178	34.6

TABLE 2. Transient orientation parameters

duration of the experiments. For $r_p = 16.9$ and $nL^3 = 10$, the population size for $\tau = 1$ was about 600, while for $\tau = 20$ the population size was only 300. In the absence of any theoretical results for $\langle C_b(t)\,C_b(t-\tau)\rangle$ we fit the data with a simple exponential function. The function $b + a\,e^{-\tau/\tau_c}$ was fitted to these data, with a and b being defined as $\langle C_b(t)^2\rangle - \langle C_b(t)\rangle^2$ and $\langle C_b(t)\rangle^2$ respectively, and τ_c determined from a best fit of the decay. All of the data sets displayed a behaviour that could be approximated by a simple exponential decay. The experimental data from the most concentrated suspensions were not resolved by as many points in the quickly decaying part of the curve, since approximately the same sampling time was used for a system with a shorter correlation time.

The correlation time, τ_c, is defined as the time required for the correlation function to decay to 1/e of its initial value. The values of $\langle C_b(t)^2\rangle$, $\langle C_b(t)\rangle^2$ and the correlation time non-dimensionalized by $\dot{\gamma}$ are shown in table 2; the correlation time is plotted as a function of concentration in figure 13 and compared with A/nL^3 using a best value of $A = 270$. The correlation time is a maximum for the lowest concentration and a minimum for the highest concentration, which was expected since the interaction rate is proportional to concentration. The values of correlation time for both aspect ratios fall on the same curve. The concentration dependence suggests

that interactions are not strongly screened in simple shear flow. This may be contrasted with Shaqfeh & Koch's (1990) results in extensional flow, which showed that interactions were increasingly screened with growing nL^3.

A possible explanation for the correlation time being independent of aspect ratio follows. Since the average projection of a fibre in the gradient direction, $\langle|p_2|\rangle$, is $O(1/r_e)$, the average amplitude of the velocity disturbance caused by a fibre goes like $1/r_e$. Thus, the rate of change of the angle θ caused by interactions would be proportional to $1/r_e$. The spacing between orbits in the (x,z)-plane goes like $1/r_e$, as can be seen from (1.7). Therefore, the increase in the rate of change of θ, caused by interactions, for the lower-aspect-ratio particles may be offset by the greater angular distance between the orbits so that the correlation time is not strongly dependent on r_e.

4. Conclusions

The complete steady-state orientation-distribution function of fibres suspended in a Newtonian fluid subjected to a nearly linear simple shear flow has been measured for several concentrations in the semi-dilute regime. A suspension of clear particles with the same refractive index as the continuous phase and one opaque tracer fibre was sheared in a Couette device, and the orientation of the tracer particle was recorded periodically. From the recorded orientations, time-average ϕ- and C-distribution functions were constructed for two different aspect ratios. For the low-aspect-ratio particles, $r_p = 16.9$ and $nL^3 = 20$, 10, 3.0, and 1.0; and for the high-aspect-ratio ones, $r_p = 31.9$ and $nL^3 = 45$, 18, 10, and 5.0.

For all the concentrations, the particles rotated around the z-axis and spent a fraction of time of about $(1-1/r_e)$ nearly aligned with the (x,z)-plane. The ϕ-distributions were similar to those predicted from Jeffery's equations. The measured C-distributions were all quite similar to one another and markedly different from the dilute C-distributions measured by Anczurowski & Mason (1967*b*). The dilute distributions heavily favour lower orbit constants, while the semi-dilute C-distributions were more uniformly distributed. An anisotropic, weak rotary diffusivity superimposed on the Jeffery convective motion (Rahnama *et al.* 1992) was shown to describe both the dilute (Anczurowski & Mason 1967*b*) and semi-dilute C-distributions with $D_{\theta\theta}/D_{\phi\phi} \approx 17$ in the dilute regime and $D_{\theta\theta}/D_{\phi\phi} \approx 1.5$ in the semi-dilute regime.

Effective viscosities measured by Bibbo (1987) in the semi-dilute regime were in qualitative agreement with those calculated from Shaqfeh & Fredrickson's (1990) semi-dilute theory using the value of $\langle p_1^2 p_2^2\rangle$ determined in this study. This agreement was improved when the factor calculated to describe the effect of finite-aspect-ratio particles in the dilute regime was used for the semi-dilute theory. Changes in the C-distribution between the dilute and semi-dilute regime have a larger influence on the effective viscosity than the small spread of the ϕ-distribution. The weakness of the observed effects of fibre interactions and the good comparison of Shaqfeh & Fredrickson's theory with measured shear viscosities suggest that fibre–fibre contact is not significant in the semi-dilute regime. The time correlation function of C_b, $\langle C_b(t)\, C_b(t-\tau)\rangle$, was fit to an exponential decay, and for all of the suspensions examined the correlation time, τ_c, was independent of aspect ratio and approximately proportional to $1/(nL^3)$.

The authors gratefully acknowledge the financial support of the members of the Cornell Injection Molding Program's industrial consortium. D.L.K. also acknowledges support from Rohm and Haas Company. Garrett Grega and Bill Park were helpful in the collection and analysis of the data. The experiments were performed in new laboratories made possible by generous gifts from H. D. Doan and the Dow Chemical Company.

REFERENCES

ANCZUROWSKI, E., COX, R. G. & MASON, S. G. 1967 *J. Colloid Interface Sci.* **23**, 547.

ANCZUROWSKI, E. & MASON, S. G. 1967*a* *J. Colloid Interface Sci.* **23**, 522.

ANCZUROWSKI, E. & MASON, S. G. 1967*b* *J. Colloid Interface Sci.* **23**, 533.

BATCHELOR, G. K. 1971 *J. Fluid Mech.* **46**, 813.

BIBBO, M. A. 1987 Rheology of semi-concentrated fiber suspensions. Ph.D. thesis, Department of Chemical Engineering, Massachusetts Institute of Technology.

BRETHERTON, F. P. 1962 *J. Fluid Mech.* **14**, 284.

BURGERS, J. M. 1938 *Second Report on Viscosity and Plasticity*, chapter 3. *Kon. Ned. Akad. Wet. Verhand.* (Eerste Sectie) **16**, 113.

CATES, M. E. & EDWARDS, S. F. 1984 *Proc. R. Soc. Lond.* A **395**, 89.

COHEN, C. & LEAL, L. G. 1978 *J. Chem. Phys.* **68**, 5348.

EVANS, J. G. 1975 The flow of a suspension of force-free rigid rods in a Newtonian fluid. Ph.D. thesis, Department of Applied Mathematics and Theoretical Physics, Cambridge University.

FOLGAR, F. & TUCKER, C. L. 1984 *J. Reinf. Plastics Composites* **3**, 98.

FRATTINI, P. L., SHAQFEH, E. S. G., LEVY, J. L. & KOCH, D. L. 1991 *Phys. Fluids* A **3**, 2516.

GANANI, E. & POWELL, R. L. 1986 *J. Rheol.* **30**, 995.

JEFFERY, G. B. 1922 *Proc. R. Soc. Lond.* A **102**, 161.

KARNIS, A., GOLDSMITH, H. L. & MASON, S. G. 1966 *Can. J. Chem. Engng* **44**, 181.

KOCH, D. L. 1989 *Phys. Fluids* A **1**, 1742.

KOCH, D. L. & SHAQFEH, E. S. G. 1990 *Phys. Fluids* A **2**, 2093.

LEAL, L. G. & HINCH, E. J. 1971 *J. Fluid Mech.* **46**, 685.

MEWIS, J. & METZNER, A. B. 1974 *J. Fluid Mech.* **62**, 593.

RAHNAMA, M., KOCH, D. L. & SHAQFEH, E. S. G. 1992 The effect of particle interactions on fiber orientation in simple shear flow of dilute and semi-dilute suspensions. *Phys. Fluids* A (to be submitted).

RALLISON, J. M. & LEAL, L. G. 1981 *J. Chem. Phys.* **74**, 4819.

SHAQFEH, E. S. G. 1988 *Phys. Fluids* **31**, 2405.

SHAQFEH, E. S. G. & FREDRICKSON, G. H. 1990 *Phys. Fluids* A **2**, 7.

SHAQFEH, E. S. G. & KOCH, D. L. 1988 *Phys. Fluids* **31**, 728.

SHAQFEH, E. S. G. & KOCH, D. L. 1990 *Phys. Fluids* A **2**, 1077.

STASIAK, W. & COHEN, C. 1983 *J. Chem. Phys.* **79**, 5718.

STOVER, C. A. 1991 The dynamics of fibers suspended in shear flows. Ph.D. thesis, School of Chemical Engineering, Cornell University.

STOVER, C. A. & COHEN, C. 1990 *Rheol. Acta* **29**, 192.

TREVELYAN, B. J. & MASON, S. G. 1951 *J. Colloid Sci.* **6**, 354.